

THE KINEMATICS IN THE CORE OF THE LOW SURFACE BRIGHTNESS GALAXY DDO 39

R. A. SWATERS^{1,2}, M. A. W. VERHEIJEN^{3,4}, M. A. BERSHADY³, D. R. ANDERSEN⁵
The Astrophysical Journal, draft version October 29, 2018

ABSTRACT

We present a high resolution, SparsePak two-dimensional velocity field for the center of the low surface brightness (LSB) galaxy DDO 39. These data are a significant improvement on previous HI or H α long slit data, yet the inner rotation curve is still uncertain due to significant noncircular and random motions. These intrinsic uncertainties, probably present in other LSB galaxies too, result in a wide range of inner slopes being consistent with the data, including those expected in cold dark matter (CDM) simulations. The halo concentration parameter provides a more useful test of cosmological models than the inner slope as it is more tightly constrained by observations. DDO 39's concentration parameter is consistent with, but on the low end of the distribution predicted by CDM.

Subject headings: galaxies: dwarfs — galaxies: halos — galaxies: kinematics and dynamics

1. INTRODUCTION

Because low surface brightness (LSB) galaxies are most likely dominated by dark matter at all radii (e.g., de Blok & McGaugh 1997; Verheijen 1997; Swaters, Madore, & Trehwella 2000), they are ideal for studying the power law slopes of the central dark matter density distributions $\rho(r) \propto \rho^{-\alpha}$. Cosmological simulations indicate α depends on the nature of the dark matter (e.g., Navarro, Frenk, & White 1997, hereafter NFW; Fukushige & Makino 1997; Moore et al. 1999; Colín, Avila-Reese, & Valenzuela 2000; Davé et al. 2001; Knebe et al. 2001). Thus, a measurement of α may provide constraints on the nature of dark matter in galaxies and theories of galaxy formation.

Unfortunately, it is difficult to measure the inner slope α observationally. HI observations have relatively low angular resolution and are affected by beam smearing (Swaters 1999, hereafter S99; Swaters et al. 2000; van den Bosch et al. 2000; McGaugh, Rubin, & de Blok 2001); hence HI observations generally are less suited to measure α accurately. H α long-slit observations provide higher angular resolution, but studies based on such observations find conflicting results. Some find LSB galaxies are consistent with steep inner slopes (Swaters 2001; Swaters et al. 2003, hereafter SMvdBB), yet others find them inconsistent with steep slopes (de Blok et al. 2001a,b; de Blok & Bosma 2002, hereafter dBB; Marchesini et al. 2002). This inconsistency remains even when identical datasets are used (SMvdBB). The apparent discrepancy can be explained, in part, by systematic effects of slit width, seeing, slit offsets and galaxy inclination, which all lead to an underestimate of α (SMvdBB).

To avoid systematic effects of long-slit observations, and to map possible non-circular motions, it is necessary to obtain high spatial resolution, two-dimensional velocity fields (see also Beauvais & Bothun 1999). Blais-Ouellette et al. (2001) presented such observations for the dwarf LSB galaxies NGC 3109 and IC 2574. Unfortunately, both galaxies are less suited to address the core issue; NGC 3109 is close to edge-on, and IC 2574 has a poorly sampled velocity field and a perturbed interstellar medium (Walter & Brinks 1999).

In this Letter, we present a high-resolution, two-dimensional

velocity field of the LSB galaxy DDO 39. This galaxy was selected because of its suitable inclination of 49° , low surface brightness ($\mu_B = 24.4$ mag arcsec⁻², Swaters & Balcells 2002), disk dominated radial surface brightness profile with a disk scale length of $h = 3.5$ kpc at an adopted distance of 12.8 Mpc (S99), regular optical and HI morphology, and well-behaved HI kinematics (see Fig. 1). These properties make DDO 39 an ideal galaxy to study the kinematics in the central regions of an LSB galaxy.

2. OBSERVATIONS AND DATA REDUCTION

DDO 39 was observed with the SparsePak integral field unit on the 3.5m WIYN telescope on January 11, 12 and 13, 2002. SparsePak is a fiber-optic array containing 82 fibers, each $4.7''$ in diameter and separated by $5.6''$, arranged in a sparsely packed grid, $72''$ on each side, with a small, nearly-integral core. Seven sky fibers are spaced between $60''$ and $90''$ away from the central fiber. The grid can be fully sampled in three pointings. For a detailed description, see Bershadly et al. (in preparation). The fibers are fed to the WIYN Bench Spectrograph. We used the 860 l/mm grating in second order at 6600 Å, yielding a FWHM velocity resolution of 66 km s⁻¹. In the first two nights we filled the grid with three 3×20 min integrations; in the third night we integrated 3×1 hour on the central pointing.

The IRAF dohydra package was used for data reduction and extraction of the spectra. Sky subtraction was done by creating a two-dimensional image of extracted spectra, filtering out the H α lines, and subtracting a low order baseline (Bershadly et al, in preparation). To determine the actual telescope pointing and offsets, we calculated the expected relative continuum flux for all fibers from an *R*-band image of DDO 39, and compared this to our observations. By minimizing the χ^2 difference, the pointing offsets could be determined with an accuracy of $\sim 0.5''$ (Swaters et al., in preparation).

We constructed a sparse velocity field by fitting Gaussians to spectra with H α emission stronger than three times the noise level and placing the derived velocities in a map at the corresponding positions. To construct a contiguous velocity field

¹ Department of Physics and Astronomy, Johns Hopkins University, 3400 N. Charles Str., Baltimore, MD 21218, and Space Telescope Science Institute, 3700 San Martin Dr., Baltimore, MD 21218. ² Visiting Astronomer, Kitt Peak National Observatory, National Optical Astronomy Observatory, which is operated by the Association of Universities for Research in Astronomy, Inc. (AURA) under cooperative agreement with the National Science Foundation. The WIYN Observatory is a joint facility of the University of Wisconsin-Madison, Indiana University, Yale University, and the National Optical Astronomy Observatory. ³ Astronomy Department, University Wisconsin - Madison, 475 N. Charter St., Madison, WI 53706. ⁴ Astrophysikalisches Institut Potsdam, An der Sternwarte 16, 14482 Potsdam, Germany. ⁵ Max Planck Institut für Astronomie, Königstuhl 17, 69117 Heidelberg, Germany

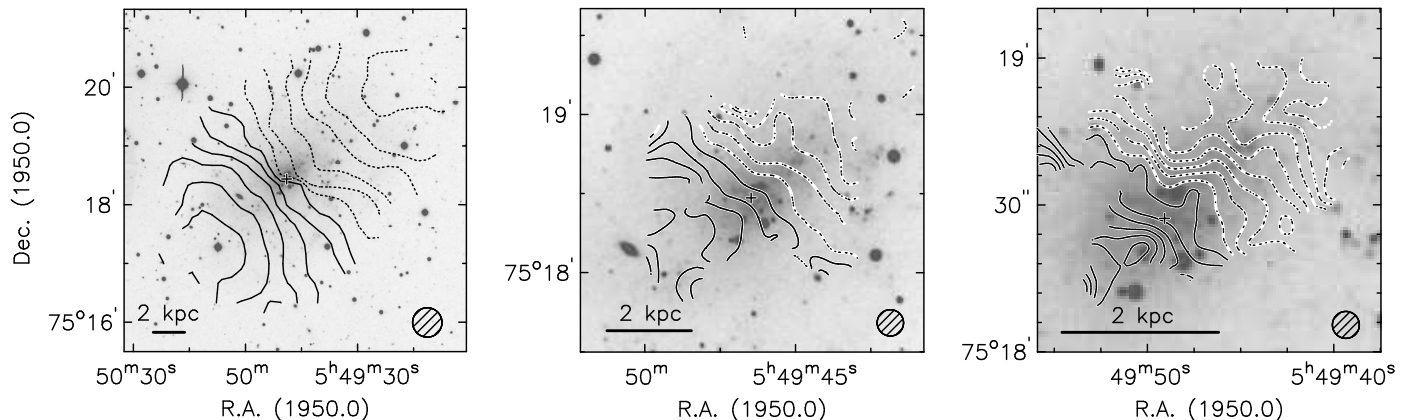


FIG. 1.— HI velocity field from Swaters et al. (2002) (left panel), SparsePak $10''$ velocity field (middle panel), and SparsePak $5.5''$ velocity field (right panel) superposed on the optical image from Swaters & Balcells (2002). Steps between isovelocity contours are 10 km s^{-1} in the left two panels, and 5 km s^{-1} in the right panel. The dotted lines represent the approaching side, the first full line indicates the systemic velocity. The beam size is given in the lower right of each panel, the cross indicates the galaxy center. Most bright objects are foreground stars.

for graphical presentation, the points in the sparse velocity field were interpolated after weighting with a Gaussian beam of $5.5''$ and $10''$. These velocity fields, shown in Fig. 1, highlight the kinematics in the central regions and over the entire SparsePak field of view. Because of the interpolation, the isovelocity contours may be uncertain, especially at the edges.

3. RESULTS

3.1. The rotation curve

To determine the galaxy orientation parameters, we fitted a tilted ring model to the sparse velocity field. Because of the approximately linear rise of the rotation curve (RC), it was not possible to determine the center or the inclination kinematically from the SparsePak data. Instead, we used the optical center at $5^{\text{h}}56^{\text{m}}37.5^{\text{s}} 75^{\circ}18'56''$ (J2000). Although the inner rotation curve shape depends somewhat on the choice of center, the main results of this Letter do not. For the inclination we used 49° , derived from the HI observations. The position angle and systemic velocity were found to be consistent with the 133° and 818 km s^{-1} of the HI observations, and we used the latter.

With these orientation parameters, all points in the sparse velocity field were corrected for projection effects. To determine the rotation velocity, points were averaged in concentric annuli with a width of $5''$. Each point was assigned a weight of $(\cos \phi / \sigma_{\text{rad}})^2$, where ϕ is the angle in the plane of the galaxy with respect to the major axis, and σ_{rad} is the error on the radial velocity, with an imposed minimum of 4 km s^{-1} . The error on the rotation velocity was taken to be the quadratic sum of the formal error and one fourth of the difference between the approaching and receding sides, with an imposed minimum error of 2 km s^{-1} . The RC derived in this way was combined with the HI RC from S99 to create the hybrid RC shown in Fig. 2a.

Fig. 2a shows good agreement between our RC and the RC derived by S99 from HI data. Fig. 2b compares dBB’s long-slit data and our data within $2.5''$ of the major axis. There is good general agreement, although the velocities derived by dBB tend to be somewhat closer to the systemic velocity. Fig. 2c compares our RC to the one derived by dBB. Although consistent within the errors, their RC is substantially lower where independent optical data are used (dBB also used S99’s data beyond $\sim 90''$). The reason for this is unclear, but the fact that we used two-dimensional data and dBB spline-interpolated their binned

data to derive their RC are both likely to play a role.

3.2. Noncircular motions

Above we have assumed that the gas moves on circular orbits. However, the $\text{H}\alpha$ velocity fields in Fig. 1 reveal significant noncircular motions. Because the velocity fields might be affected by interpolation, we have also plotted the data directly. In Fig. 3 we plot the observed radial velocities with respect to systemic velocity in different radial intervals, normalized by the rotation velocity. At large radii the radial velocities follow the curve expected for circular rotation closely. On the other hand, in the innermost regions there are clear deviations from simple circular motions.

Fig. 3 also shows that there is significant scatter around the best fit rotation velocity. The scatter (before normalization) is around 9 km s^{-1} , independent of radius. The scatter is in part due to observational uncertainties. Measurement errors depend on the signal-to-noise ratio and range from 2 to around 8 km s^{-1} for the weakest lines, and average about 4 km s^{-1} . Additional scatter may arise if the intensity weighted position of the $\text{H}\alpha$ over the fiber “beam” does not coincide with the center of that fiber. The maximum contribution of this effect, modeled by calculating the extreme velocities in each fiber and comparing those to the expected velocities, is found to be lower than 3 km s^{-1} at all radii. Subtracting the dominant sources of observational uncertainties from the observed dispersion in the rings, we find the intrinsic fiber-to-fiber line-of-sight dispersion is around 8 km s^{-1} .

Because the dispersion σ is comparable to the rotation velocity v_{ϕ} in the central regions, it may be necessary to correct the RC to obtain the circular velocity. If one assumes the dispersion represents pressure support due to random motions, then, assuming axisymmetry and absence of radial motions, the correction can be calculated and is found to be negligible (see e.g., S99). Alternatively, if one assumes the central regions are in a steady state, one can calculate the circular velocity v_c using the virial theorem, $2T + \Pi = W$. Although the kinetic energy in rotation T and in random motions Π depend on the distribution of the gas, and the gravitational potential W depends on the total mass distribution, comparison to more detailed calculations

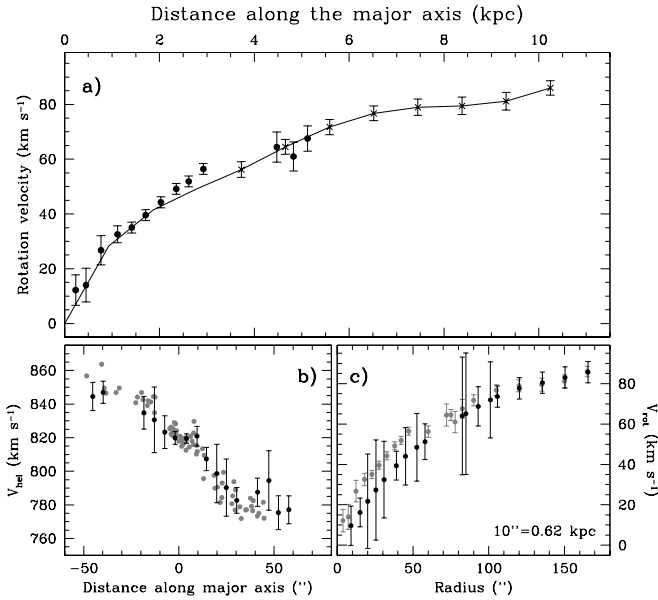


FIG. 2.— **a)** Hybrid rotation curve from SparsePak data (*dots*) and the HI data from S99 (*crosses*). The rotation curve from S99 is given by the solid line. **b)** Comparison of dBB’s data (*black dots*) to SparsePak data within $2.5''$ of the major axis (*grey dots*). **c)** Comparison of dBB’s and our rotation curve, coding as in panel b.

show the circular velocity is approximately equal to:

$$v_c^2 = v_\phi^2 + \beta\sigma^2. \quad (1)$$

Assuming an isotropic dispersion ($\beta = 3$) results in a steeper RC (see Fig. 5).

Because the origins of the dispersion and noncircular motions are not known, and because the assumptions for the corrections may not be valid, these corrections are uncertain and merely give an indication of the possible range.

3.3. Mass models

The contribution of the stellar disk to the RC was calculated from the R -band light profile presented in Swaters & Balcells (2002), and the contribution of HI was calculated from the HI surface density profile presented in Swaters et al. (2002), scaled up by a factor of 1.32 to account for helium. The stellar disk was assumed to have a vertical sech-squared distribution with a scale height $z_0 = h/6 = 0.58$ kpc, and the HI disk was assumed to be infinitely thin. For the dark matter halo we considered a generalized NFW halo of the form:

$$\rho(r) = \frac{\rho_0}{(r/r_s)^\alpha (1+r/r_s)^{3-\alpha}}, \quad (2)$$

where r_s is the scale radius and ρ_0 the central density. These two parameters are linked to the more commonly used parameters c and v_{200} , depending on cosmology (see Section 4).

We have fit mass models over a range of α and mass-to-light ratios (M/Ls). In each fit α and the M/Ls were kept fixed and the halo parameters were allowed to vary. Confidence levels were not calculated because the velocities and their errors are not free of systematic effects, and hence the χ^2 values were only used for relative comparison between the models. In Fig. 4 we plot the resulting χ_r^2 values as a function of α for an M/L of 1. Fits to the uncorrected and pressure corrected RCs give virtually identical results, with best fits in the range $0 < \alpha \lesssim 0.8$. For

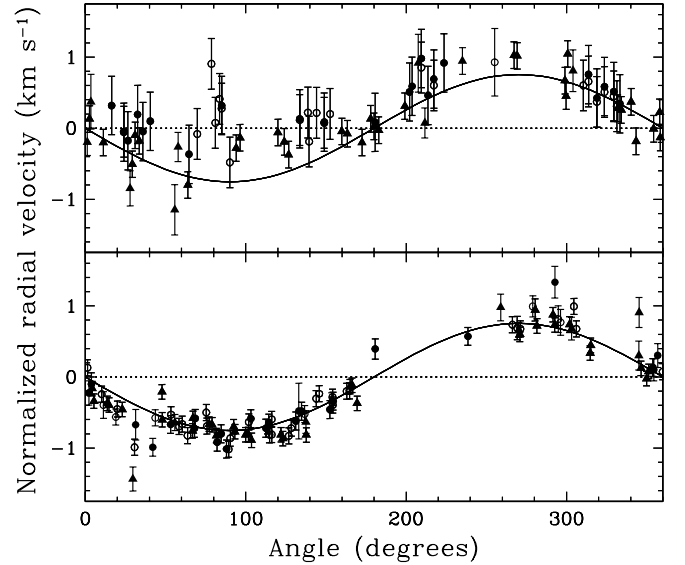


FIG. 3.— Radial velocity with respect to the systemic velocity, normalized by the rotation velocity, as a function of angle in the plane with respect to the minor axis. The dots, circles and triangles represent the points at radii of 0.23, 0.45, and 0.77 kpc in the top panel, and 1.71, 2.03, and 2.35 kpc in the bottom panel, respectively. The solid line represents the normalized curve for circular rotation.

the RC corrected using the virial theorem, best fits are found for somewhat steeper inner slopes, in the range $0.3 \lesssim \alpha \lesssim 1.0$. For higher values of α the quality of the fits decreases rapidly.

Best fitting mass models for an M/L of 1 are shown in Fig. 5, for $\alpha = 1$ (the NFW profile) and $\alpha = 0$. The difference between the $\alpha = 0$ and $\alpha = 1$ models are predominantly in the inner 1 kpc, where the RC is most affected by noncircular and random motions (Fig. 5). The best fitting parameters for a range of M/Ls and $\alpha = 1$ are given in Table 1, both for the pressure corrected RC and the one corrected with Eq. 1 and $\beta = 3$.

4. DISCUSSION AND CONCLUSIONS

The high-resolution velocity field of the LSB galaxy DDO 39 presented here reveals the presence of noncircular motions in the central regions and an intrinsic fiber-to-fiber dispersion of about 8 km s^{-1} . The origin of either component is unclear; DDO 39 does not have a strong bar or spiral arms, nor does it appear to be interacting. Likely contributors are: star formation activity, turbulence, and small scale structure in the disk or dark halo. Irrespective of their origin, the noncircular motions and the large σ/v_ϕ in the galaxy center make an accurate measurement of the circular velocity curve difficult.

As a result, inner slopes in the range $0 < \alpha \lesssim 1$ are consistent with the data, and DDO 39 is compatible with a wide range of dark matter properties. Specifically, it appears that the data presented here are consistent with the inner slopes expected in the currently popular Λ CDM paradigm. Although earlier simulations predicted inner slopes ranging from $\alpha = 1.5$ (e.g., Fukushige & Makino 1997, Moore et al. 1999) to $\alpha = 1$ (e.g., NFW), a recent study by Power et al. (2003) suggests that the differences in α are mainly due to resolution issues, and places an upper limit to α of 1.2. Taylor & Navarro (2001), based on analytical arguments, find α may be as low as 0.75 at very small radii.

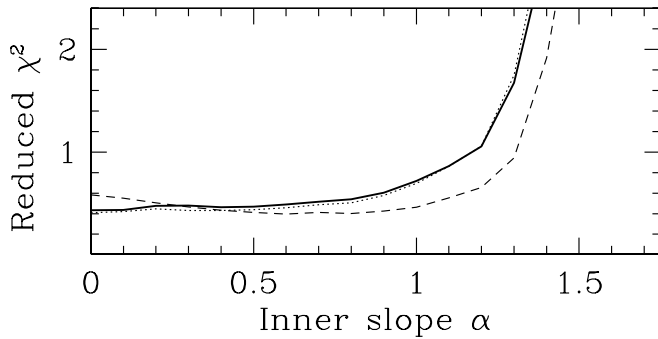


FIG. 4.— χ_r^2 versus α , as determined from fits with M/L fixed to 1, and the halo parameters left free. The full line gives the results for fits to the uncorrected rotation curve, the dotted line for pressure correction, and the dashed line for the virial correction of Eq. 1.

TABLE 1
BEST FIT PARAMETERS FOR $\alpha = 1$

Υ_*^R	NFW (pressure)			NFW (virial)		
	c	v_{200} (km s $^{-1}$)	χ_r^2	c	v_{200} (km s $^{-1}$)	χ_r^2
0	6.1	90	0.77	7.1	83	0.51
1	4.4	93	0.72	5.6	83	0.46
2	2.1	148	0.75	4.0	92	0.44
4	1.0	150	0.81	1.4	143	0.46
1	10 ^a	54	4.0	10 ^a	54	2.6

Note — ^a Fit with c fixed

Even though the data presented here eliminate several uncertainties that gave poor constraints on α from HI and H α longslit observations (van den Bosch et al. 2000, van den Bosch & Swaters 2001, SMvdBB, but see de Blok et al. 2001a,b), the intrinsic noncircular and random motions still result in poor constraints on α . Given that deviations from circular motions seem common in LSB galaxies (e.g., Walter & Brinks 1999, de Blok & Walter 2000), and are present even in a very LSB galaxy such as DDO 39, it seems that an accurate measurement of α and, from that, a tight limit on the nature of dark matter may be difficult to achieve observationally from a component that is susceptible to kinematic perturbations.

Fortunately, the halo concentration parameter c is better constrained observationally as it is derived from a fit to the RC as a whole rather than mostly from the central parts, although it may still be affected by systematic effects (SMvdBB). For the case of $\alpha = 1$, the inferred halo parameters c and v_{200} can be

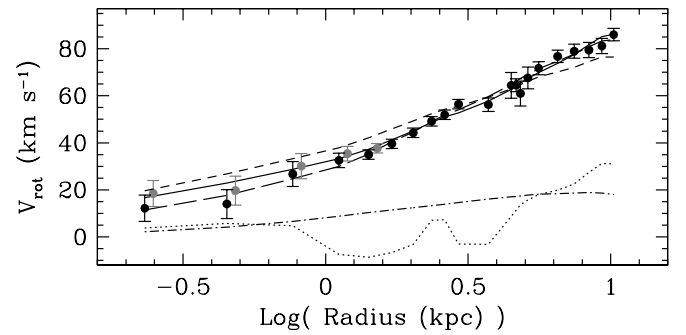


FIG. 5.— Mass models for the best fit NFW halo (solid line), for an NFW halo with $c = 10$ (short dashed line), and for a halo with $\alpha = 0$ (long dashed line). The dotted line represents the contribution of the HI, the dot dashed line the contribution of the stars with an M/L of 1. The contribution of the halo is similar to the best fit model, but is not shown. The black dots give the uncorrected rotation curve, the gray dots (only shown for the inner five points and offset by 0.03 for clarity) represent the rotation curve corrected using Eq. 1 assuming $\beta = 3$.

compared to the values expected in a Λ CDM cosmology. Expected values have a 2σ range from 5 to 25, with an average of around 10 to 15 (NFW, Bullock et al. 2001). DDO 39's $c \sim 5$ is at the low end of this distribution, and for different values of c the quality of the fit changes rapidly. For example, $c = 10$ is inconsistent with the data (see Fig. 5 and Table 1).

The low value for c does not necessarily indicate an inconsistency with Λ CDM. For example, a bias toward low c values in LSB galaxies could be explained if LSB galaxies preferentially form in low density halos. In addition, the concentration parameter also depends on the slope of the power spectrum of density fluctuations, and $c \sim 5$ is in agreement with models in which structure formation on small scales is suppressed (Zentner & Bullock 2002). Furthermore, c would be higher if DDO 39 were closer than the adopted 12.8 Mpc.

Accurate RCs determined from high resolution, two-dimensional velocity fields for a sample of LSB galaxies with intermediate inclinations, accurate centers, and regular kinematics and morphology may provide RCs to measure c , or any parameter that depends on the global shape of the RC, with sufficient accuracy to provide useful constraints on the nature of dark matter.

This research was supported in part from NSF grant AST-9970780.

REFERENCES

- Beauvais, C. & Bothun, G. 1999, ApJS, 125, 99
Colin, P., Avila-Reese, V., & Valenzuela, O. 2000, ApJ, 542, 622
Davé, R., Spergel, D. N., Steinhardt, P. J., & Wandelt, B. D. 2001, ApJ, 547, 574
de Blok, W. J. G., & Bosma, A. 2002, A&A, 385, 816 (dBB)
de Blok, W. J. G. & McGaugh, S. S. 1997, MNRAS, 290, 533.
de Blok, W. J. G. & Walter, F. 2000, ApJ, 537, L95
de Blok, W. J. G., McGaugh, S. S., Bosma, A., & Rubin, V. C. 2001, ApJ, 552, L23
de Blok, W. J. G., McGaugh, S. S., & Rubin, V. C. 2001, AJ, 122, 2396
Bullock, J. S., Kolatt, T. S., Sigad, Y., Somerville, R. S., Kravtsov, A. V., Klypin, A. A., Primack, J. R., & Dekel, A. 2001, MNRAS, 321, 559
Fukushige, T., & Makino, J. 1997, ApJ, 477, L9
Knebe, A., Devriendt, J., Mahmood, A., & Silk, J. 2001, astro-ph/0105316
Marchesini, D., D'Onghia, E., Chincarini, G., Firmani, C. Conconi, P., Molinari, E., & Zacchei, A. 2002, ApJ, 575, 801
McGaugh, S. S., Rubin, V. C., & de Blok, W. J. G. 2001, AJ, 122, 2381
Moore, B., Quinn, T., Governato, F., Stadel, J., & Lake, G. 1999, MNRAS, 310, 1147
Navarro, J. F., Frenk, C. S., & White, S. D. M. 1997, ApJ, 490, 493
Power, C., et al., 2003, MNRAS, 338, 14
Swaters, R. A. 1999, PhD thesis, Rijksuniversiteit Groningen (S99)
Swaters, R.A. 2001, in: Galaxy Disks and Disk Galaxies, eds. J.G. Funes S.J., E.M. Corsini, ASP conf. series 230, p. 545
Swaters, R. A., Balcells, M. 2002, 390, 863
Swaters, R. A., Madore, B. F., & Trewheella, M. 2000, ApJ, 531, L107
Swaters, R. A., van Albada, T. S., van der Hulst, J. M., & Sancisi, R. 2002, \hat{a} , 390, 829
Swaters, R. A., Madore, B. F., van den Bosch, F. C., Balcells, M., ApJ, in print
Taylor, J. E. & Navarro, J. F. 2001, ApJ, 563, 483
van den Bosch, F. C. & Swaters, R. A. 2001, MNRAS, 325, 1017
van den Bosch, F. C., Robertson, B. E., Dalcanton, J. J., & de Blok, W. J. G. 2000, AJ, 119, 1579
Verheijen, M. A. W. 1997, PhD thesis, Rijksuniversiteit Groningen
Walter, F. & Brinks, E. 1999, AJ, 118, 273
Zentner, A. R. & Bullock, J. S. 2002, Phys. Rev. D, 66, 43003